

# Dynamics of charged particles and quasi-periodic oscillations in the vicinity of a distorted, deformed compact object embedded in a uniform magnetic field

Shokoufe Faraji\* and Audrey Trova†

*University of Bremen, Center of Applied Space Technology and Microgravity (ZARM), 28359 Germany*

This work presents the dynamic properties of charged test particles influenced by the gravitational and electro-magnetic fields. Accordingly in this work, we concentrate on the static and axially symmetric metric containing two quadrupole parameters. One relates to the central object, and another relates to the external distribution of matter. This metric may associate the observable effects to these parameters as dynamical degrees of freedom. The astrophysical motivation for choosing such a field is the possibility to constitute a reasonable model for an actual situation occurring in the objects' vicinity. To test the role of large-scale magnetic fields in accretion processes, we start by analyzing different bound orbits of timelike orbits under the influence of the system's different parameters. This leads to examining their stability concerning radial and/or vertical oscillations. The main focus is to discuss the effect of magnetic field on the oscillation modes' resonant phenomena using different resonant models for disc-oscillation modes. In the present contribution, we further explore the possibility of relating oscillatory frequencies of charged particles to the frequencies of the high-frequency quasi-periodic oscillations observed in the microquasars GRS 1915+105, XTE 1550-564 and GRO 1655-40 via assuming relevance of resonant phenomena of the radial and vertical oscillations.

## I. INTRODUCTION

There is no doubt on the role of the magnetic fields in the study of astrophysical systems. In the processes occurring in the vicinity of compact objects, the magnetic fields can manifest their fingerprint in many ways. For example, the local magnetic field in the thin accretion disc is assumed to be the source of viscosity in the accretion process in MRI simulations [1]. In fact, many black hole candidates are believed to have an accretion disc forming from conducting plasma which their dynamics can produce magnetic fields e.g. [2–4].

An external magnetic field at a large distance in a finite region can be approximated as a uniform magnetic field [5, 6]. Such a large-scale magnetic field could be initiated during the early phases of the expansion of the Universe [7–11]. Further, a compact object near the equatorial plane of a magnetar can be approximated to be in a uniform magnetic field if the magnetar is at a distance large enough [12, 13]. In fact, the motion in a gravitational field and in the presence of an external electromagnetic field was explored in a large variety of studies e.g. [14–16] among many more. In this respect, the fundamental frequencies of the motion of test particles play a crucial role in several important astrophysical phenomena. In particular, these frequencies are considered within a great deal of attempts to explain the existence of high-frequency peaks in the Fourier power spectra of X-ray radiation from accreting compact sources and predict lower and upper frequencies of their pairs  $(\nu_U, \nu_L)$ .

The so far unexplained rapid variability (so-called high-frequency quasi periodic oscillations - HF QPOs) is usually supposed to originate from the orbital motion in the innermost parts of an accretion disk, since the peaks of high frequencies are close to the orbital frequency of the marginally stable circular orbit representing the inner edge of Keplerian discs.

This rapid variability arises across a large scale of mass of the compact sources including both neutron star and black hole low-mass X-ray binaries (LMXBs), as well as active galactic nuclei [17–24].

Among many models serving to explain QPOs in the past years is the Relativistic Precession Model (RPM). This model assumes that QPOs are produced by a local motion of accreted inhomogeneities like blobs, and relates the twin-peak QPOs to the Keplerian and periastron precession frequency on an orbit located in the inner part of the accretion disc [25, 26].

In this regard, the properties of the Keplerian and epicyclic frequencies of the orbital motion have been extensively studied in the context of particle motion underlying the presence of a uniform magnetic field in various spacetimes [6, 13, 27–38] among many others.

Although, in general, the correlation between these frequencies is qualitatively fitted by the RPM prediction [see 39, for a detailed discussion and references], the RPM suffers some theoretical difficulties to explain for example a relatively large observed HF QPO amplitudes which is often observed [40, 41]. During these years, this model modified in many ways. In 2001, the orbital resonance model was introduced. In this model it was supposed that HF QPOs arise from the resonances between oscillation modes of the accreted fluid [42, 43]. In fact, several studies within the HF QPOs framework consider fluid motion instead of a test particle motion. In this respect, a different class of models, deals with the collective motion of accreted matter considering normal modes of thin accretion disk oscillations (so-called diskoseismology) and thick disk (torus) oscillations e.g. [44–51]. In some cases, the QPO frequencies predicted by a given model can still be expressed in the test particle motion for the epicyclic oscillations of slender accretion tori or with reasonable accuracy for the consideration of discoseismic modes. In principle, it is worth mentioning that it is a rather long way from the test particle motion examination to considering the more realistic case of non-slender tori oscillations that has severe impacts on the predicted QPO frequencies e.g. [52, 53].

Although, in general, the correlation between these fre-

\* shokoufe.faraji@zarm.uni-bremen.de

† audrey.trova@zarm.uni-bremen.de

quencies is qualitatively fitted by the RPM prediction, the RPM suffers some theoretical difficulties to explain, for example, the relatively large HF QPO amplitudes that are often observed.

In this work, we explore properties of the Keplerian and epicyclic frequencies of a charged particle motion in the background of a distorted, deformed compact object with a relatively weak uniform magnetic field that does not affect the spacetime curvature in the vicinity of the compact object. This metric is the generalization of the so-called q-metric up to quadrupole moments and aside from the mass of the central object it has two parameters; namely, distortion parameter  $\beta$  and deformation parameter  $\alpha$ , which are not independent of each other. This area of study has been discussed extensively in the literature [54–59], among many others. We explain briefly about this metric in Section II.

In the present work, the effects of the electromagnetic field on the stress-energy tensor is neglected. Concerning the observable phenomena, we assume that the HF QPO frequencies can be expressed in terms of the epicyclic frequencies of the charged particle motion. Considering the presence of magnetic field along with a broader spacetime description that can deviate from the Kerr case, we aimed to explore various possibilities of explaining the observed QPOs frequencies with the 3 : 2 ratio.

Furthermore, using the Hamiltonian formalism of the charged particle dynamics, we examine bound orbits via the effective potential of the gravitational field combined with the uniform magnetic field. We are particularly curious about the dynamics regime of motion and its changes with the different combinations of parameters. In addition, we have some freedom in defining these dynamical parameters; however, this work mainly focuses on studying the effect of the magnetisation parameter.

Our survey is of particular interest for several reasons. First, it is assumed that the Schwarzschild or Kerr metrics describe astrophysical compact objects in the relativistic astrophysical study. However, besides these setups, others can imitate a black hole's properties, such as the electromagnetic signature [60]. Also, astrophysical observations may not be fitted, in general, within the general theory of relativity by using the Schwarzschild or Kerr metric [61, 62], like as the mentioned ratio of QPOs.

In addition, due to their strong gravitational field, considering astrophysical environments, compact objects are not necessarily isolated or possess spherical symmetry. In particular, it seems that the present understanding of astronomical phenomena mostly relies on studies of the stationary and axially symmetric models. It has been shown [63] that the possible resonant oscillations can be directly observed when arising in the inner parts of accretion flow around a compact object, even if the source is steady and axisymmetric.

Moreover, we believe our setup allows for the constitution of a set of various reasonable prescriptions for the QPO frequencies, and provide a possibility to study the impact of spacetime and magnetic field parameters on the predicted QPO frequencies analytically.

The paper's organization is as follows: Section II presents

the background spacetime. The dynamics of charged particles is presented in Section III. Section IV discusses epicyclic frequencies and stable circular orbits. In Section V, we briefly present QPO models and the related set of prescriptions for the QPO frequencies. In Section VI, we compare the expected QPO frequencies to the observational data. Finally, conclusions are summarized in Section VII.

Throughout this work, we use the signature  $(-, +, +, +)$  and geometrized unit system  $G = 1 = c$  (However, for an astrophysical application, we will use SI units). Latin indices run from 1 to 3, while Greek ones take values from 0 to 3.

## II. METRIC OF THE DISTORTED DEFORMED COMPACT OBJECT

The first static and axially symmetric solution of Einstein's field equation with arbitrary quadrupole moment is described by Weyl solutions [64]. Later, Zipoy and Voorhees [65, 66] introduced an equivalent transformation to  $\sigma$ -metric (or  $\gamma$ -metric) that can handle analytically. Then, by introducing a new parameter it is known as q-metric [67].

In this paper, we choose to work on the generalized version of q-metric describing a deformed compact object characterized by quadrupole, while surrounded by a static and axially symmetric external distribution of matter in its vicinity up to the quadrupole [68]. The metric has this form

$$ds^2 = -\left(\frac{x-1}{x+1}\right)^{(1+\alpha)} e^{2\hat{\psi}} dt^2 + M^2(x^2-1)e^{-2\hat{\psi}} \left(\frac{x+1}{x-1}\right)^{(1+\alpha)} \left[\left(\frac{x^2-1}{x^2-y^2}\right)^{\alpha(2+\alpha)} e^{2\hat{\gamma}} \left(\frac{dx^2}{x^2-1} + \frac{dy^2}{1-y^2}\right) + (1-y^2)d\phi^2\right], \quad (1)$$

where  $t \in (-\infty, +\infty)$ ,  $x \in (1, +\infty)$ ,  $y \in [-1, 1]$ , and  $\phi \in [0, 2\pi)$ . The function  $\hat{\psi}$  plays the role of gravitational potential, and the function  $\hat{\gamma}$  is obtained by an integration of the explicit form of the function  $\hat{\psi}$ . We consider these functions up to quadrupoles as

$$\hat{\psi} = -\frac{\beta}{2} [-3x^2y^2 + x^2 + y^2 - 1], \quad (2)$$

$$\hat{\gamma} = -2x\beta(1+\alpha)(1-y^2) + \frac{\beta^2}{4}(x^2-1)(1-y^2)(-9x^2y^2 + x^2 + y^2 - 1). \quad (3)$$

By its construction, this metric is valid locally. In fact, this metric has three parameters: the total mass  $M$ , deformation parameter  $\alpha$ , and distortion parameter  $\beta$ . These two parameters are chosen to be relatively small and connected to the q-metric and the surrounding external mass distribution, respectively [69]. For vanishing  $\beta$ , we recover the q-metric, and in the case of  $\alpha = \beta = 0$ , the Schwarzschild metric is retrieved. This metric may links the observable effects to the system due to taking these parameters as the new dynamical degrees of

freedom. In addition, we try to minimize computational time and numerical errors, since we have some freedom to choose these relatively small dynamical variables.

The relation between the prolate spheroidal coordinates  $(t, x, y, \phi)$ , and the Schwarzschild coordinates  $(t, r, \theta, \phi)$  reads as

$$x = \frac{r}{M} - 1, \quad y = \cos \theta. \quad (4)$$

In the rest of the work, we explore this space-time by analyzing the dynamics of particles motion in the presence of an asymptotically uniform magnetic field.

### III. DYNAMIC OF CHARGED PARTICLE IN A UNIFORM MAGNETIC FIELD

In this work, we consider a weak magnetic field to have no influence on the background space-time. Explicitly, we are interested in the dynamics that occur when a static, axisymmetric central compact object is embedded in an asymptotic uniform magnetic field of strength  $B$  aligned with the central body's symmetry axis, and nonsingular throughout the exterior region [70]. In general, by comparing the compact object's size with the typical length of varying the strength's electric and magnetic fields, we can define a test particle.

Furthermore, the motion of neutral test particles that is not influenced by magnetic fields satisfying

$$B_G \sim 10^{19} \left( \frac{M_\odot}{M} \right) G. \quad (5)$$

This condition comes from comparing the central body's gravitational effect and the strength of the magnetic field  $B$  on its vicinity, and for most astrophysical black holes is perfectly satisfied [71]. In addition, the relative strength of the Lorentz and gravitational forces acting on a charged particle moving in the vicinity of a black hole can be characterized by a dimensionless quantity  $b$  which is identified as the relative Lorentz force by the order of

$$b \sim 4.7 \times 10^7 \left( \frac{q}{e} \right) \left( \frac{m_p}{m} \right) \left( \frac{B}{10^8} \right) \left( \frac{M}{10M_\odot} \right), \quad (6)$$

where  $m_p$  is the mass of a proton,  $m$  and  $q$  are the mass and charge of the particle. The ratios in this quantity suggest that this characterization is relevant and cannot be neglected for the astrophysical scales.

We start our analysis by stating the standard electromagnetic tensor as

$$F_{\mu\nu} = \partial_\mu A_\nu - \partial_\nu A_\mu. \quad (7)$$

As mentioned, following [70] the external asymptotically homogeneous magnetic field is chosen to be along the polar axis and described by the  $\phi$ -component of the vector potential. In this metric  $A_\phi$  is obtained as

$$A_\phi = \frac{1}{2} B (x^2 - 1) e^{-2\hat{\psi}} \left( \frac{x+1}{x-1} \right)^{(1+\alpha)}. \quad (8)$$

The Lorentz equation that describes the charged test particle motion is given by

$$m \frac{du^\mu}{ds} = q F^\mu{}_\nu u^\nu, \quad (9)$$

where  $u^\mu = \frac{d}{ds}$  is the four-velocity of the particle and  $s$  is the affine parameter. In the following part, we use the general Hamiltonian approach to describe the effective potential and dynamics of a charged particle in the vicinity of a distorted, deformed compact object embedded in the external uniform magnetic field.

#### A. Hamiltonian and effective potential on the equatorial plane

The Hamiltonian for the charged particle motion is written as,

$$H = \frac{1}{2} \left[ (\pi^\mu - qA^\mu)(\pi_\mu - qA_\mu) + m^2 \right], \quad (10)$$

where the generalized canonical four-momentum is written in terms of four-momentum

$$\pi^\mu = p^\mu + qA^\mu. \quad (11)$$

Considering the metric is static and axisymmetric, the conserved quantities are specific energy  $E$  and angular momentum  $L$  of the particle. They express as follows

$$E = -\pi_t = \left( \frac{x-1}{x+1} \right)^{(1+\alpha)} e^{2\hat{\psi}} \frac{dt}{ds}, \quad (12)$$

$$L = \pi_\phi = (x^2 - 1) e^{-2\hat{\psi}} \left( \frac{x+1}{x-1} \right)^{(1+\alpha)} \left( \frac{d\phi}{ds} + Q \right), \quad (13)$$

where  $Q := \frac{qB}{2m}$  is magnetic parameter. In addition, the effective potential is obtained as

$$V_{\text{Eff}} = \left( \frac{x-1}{x+1} \right)^{(\alpha+1)} e^{2\hat{\psi}} \left[ \epsilon + \right. \quad (14)$$

$$\left. e^{-2\hat{\psi}} \left( \frac{x+1}{x-1} \right)^\alpha (1-y^2) \left( \frac{Le^{2\hat{\psi}}}{(x+1)(1-y^2)} \left( \frac{x-1}{x+1} \right)^\alpha - Q(x+1) \right)^2 \right].$$

The second term corresponds to the central force potential related to  $L$ , and electromagnetic potential energy related to  $B$ . In general, we can discuss four different situations in terms of signs of  $L$  and  $Q$ . However, because of the even power in the second term it is sufficient to consider only two situations:

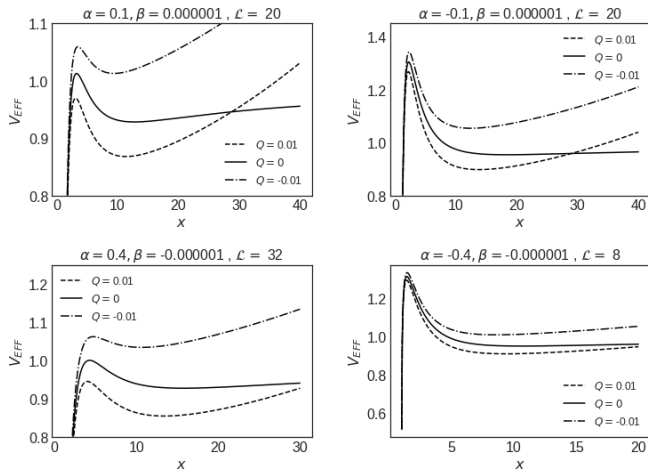


FIG. 1. Effective potential for different combinations of the model's parameters: the distortion  $\beta$ , the deformation  $\alpha$  and the magnetic parameter  $Q$ .

1.  $LQ > 0$ , the Lorentz force pushes the particle away in the outward direction with respect to the central object.
2.  $LQ < 0$ , the Lorentz force pushes the particle in the direction of the  $z$ -axis towards the central object.

Moreover, there is a shortcut in the study of the charged particles motion by analyzing the effective potential. In fact, this motion is determined by the energy's boundaries given by  $\mathcal{E} = V_{\text{eff}}$ , where  $\mathcal{E} = E^2$ . In Figure 1, the effective potential presented for different values of parameters  $\alpha$  and  $\beta$ .

In general, different types of orbit dependent on the parameters  $\epsilon$ ,  $\mathcal{E}$ ,  $L$ ,  $\alpha$ ,  $\beta$  and  $Q$  are possible. In the analytical exploration depending on the number of positive real zeros and the sign of  $\mathcal{E} - \epsilon$ , one can obtain different types of trajectories.

We chose to discuss bounded timelike trajectories in this work for their importance in studying the oscillation of particles for a small perturbation in orbit. There is no surprise that test particles' motion can be chaotic in this metric for some combinations of parameters. In fact, when particles are trapped in some region, their trajectories form a toroidal shape around the central object. Figures 2-4 present some examples of different choices. As we see in the plots, one can obtain different patterns only by a slight change in the value and sign of parameters. In particular, as the Figures 2-4 suggest, apart from the effect of other parameters, the value for  $\alpha$  makes a profound difference in the trajectories. Further analysis reveals that aside from the magnitude, the influence of the signs of magnetic parameter  $Q$  along with the sign of  $\alpha$  together, have a significant impact on the results.

#### IV. EPICYCLIC FREQUENCIES AND STABILITY OF CIRCULAR MOTION IN A UNIFORM MAGNETIC FIELD

There is no doubt on the crucial role of the circular and quasi-circular orbits in the study of accretion processes. In fact, in these processes a variety of oscillatory motions are

expected. In this regard, in the study of the relativistic accretion disc three frequencies contribute: The radial frequency  $\nu_x = \frac{\omega_x}{2\pi}$ , the vertical frequency  $\nu_y = \frac{\omega_y}{2\pi}$ , and the Keplerian orbital frequency  $\nu_K = \frac{\Omega}{2\pi}$ . Furthermore, the resonance among these frequencies may be a source of the chaotic and quasi-periodic variabilities in X-ray fluxes observations.

These fundamental frequencies in the Schwarzschild background, in spheroidal coordinates, are given by

$$\omega_y^2 = \Omega^2 = \frac{1}{(x+1)^3}, \quad (15)$$

$$\omega_x^2 = \frac{1}{(x+1)^3} \left( 1 - \frac{6}{x+1} \right). \quad (16)$$

The vertical and keplerian frequencies are positive, but it is not the case for radial frequency. Therefore, the stable circular orbits are located at radial distances larger than the location of the ISCO at  $x = 5$  in these coordinates. Besides, for the Schwarzschild solution we have  $\omega_x^2 < \omega_y^2 = \Omega^2$ . In fact, in contrast to Newtonian geometry, bounded quasi-elliptic orbits can also exist. Namely, the trajectories relevant to a perturbed stable circular test particle may not be elliptic but exhibit a periapsis shift. This is often called the effect of relativistic precession [72].

In what follows, we investigate the stability of circular motion in the presence of the asymptotically homogeneous magnetic field. In this regard, seminal papers [27, 28] studied the existence and stability of circular non-geodesic equatorial orbits, and derived Keplerian and epicyclic orbital frequencies in Kerr(-Newman) geometry. One of the particular models they considered was a rotating black hole immersed in an asymptotic uniform external magnetic field. In this work, following their method we extend the result to this space-time containing quadrupoles. Of course, if parameters of the metric vanish, the axial and radial oscillations frequencies are reduced to the ones given in their works for non-rotating case.

The equation of motion for a particle with mass  $m$  and electric charge  $e$  is the geodesic equation with force in its right-hand side reads as

$$\frac{d^2 x^\mu}{ds^2} + \Gamma_{\nu\rho}^\mu \frac{dx^\nu}{ds} \frac{dx^\rho}{ds} = \frac{q}{m} F_{\nu\eta}^\mu \frac{dx^\eta}{ds} \quad (17)$$

In the equatorial plane we have  $x = x_0$  and  $y = 0$ , and further we replaced all necessary Christoffel symbols on the left-hand side. For substitute the right hand side we use (7) and (8).

To derive a more general class of orbits in the equatorial plane deviating from the circular ones, one can use the perturbation approach and consider a slightly perturbed orbit  $x'^\mu = x^\mu + \xi^\mu$  from the original one  $x^\mu$ . By substituting this relation into equation (17) and consider only linear orders in  $\xi^\mu$ , we obtain [28]

$$\frac{d^2 \xi^\mu}{dt^2} + 2\gamma_\eta^\mu \frac{d\xi^\eta}{dt} + \xi^\eta \partial_\eta U^\mu = \frac{q}{mu^0} f^\mu, \quad (18)$$

where,

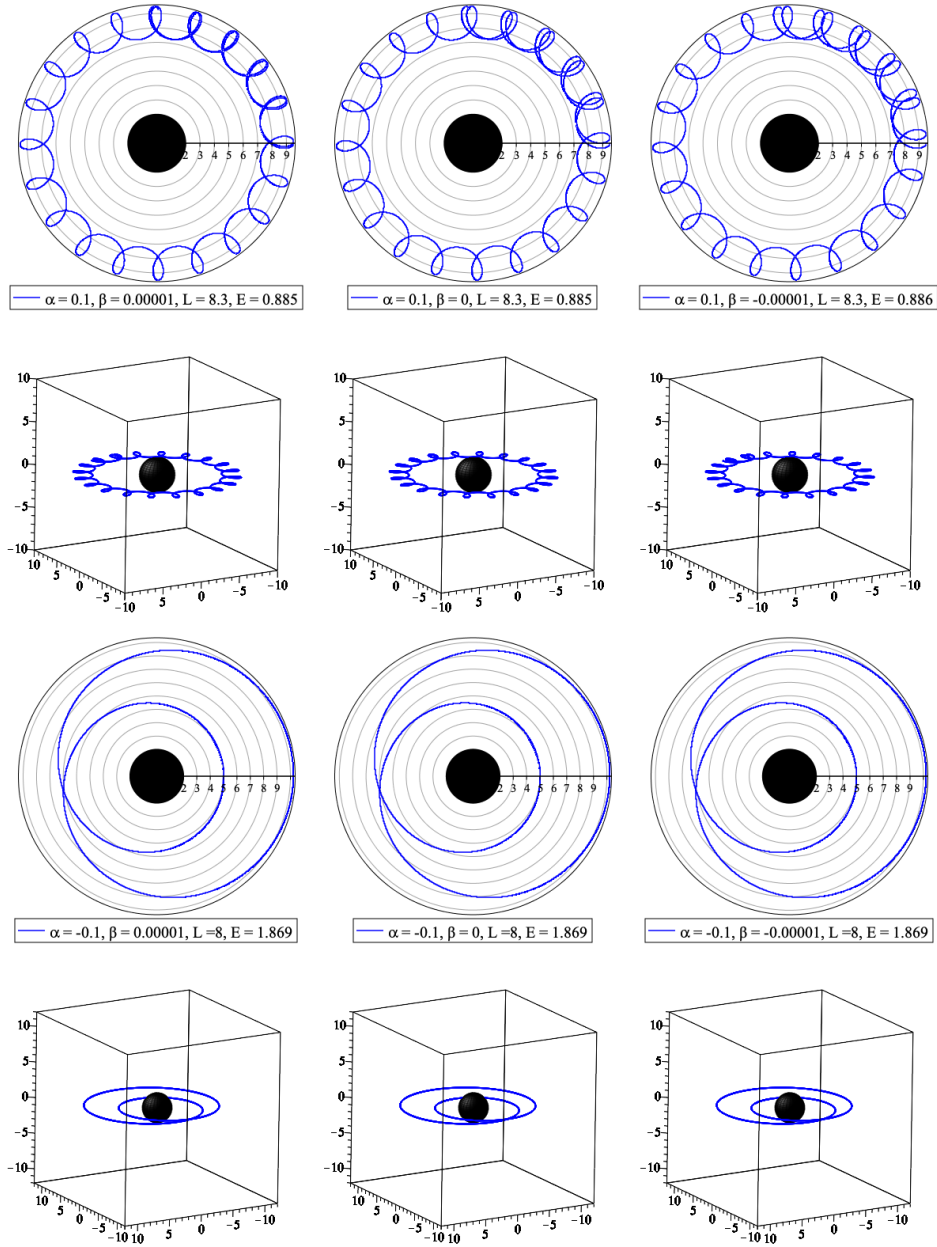


FIG. 2. Trajectories of particles for some choices of the parameters. In the first row  $Q > 0$  and  $\alpha > 0$ , and the initial radius is set to be  $r_0 = 9.5$ . In the second one  $Q < 0$  and  $\alpha < 0$ , and the initial radius is set to be  $r_0 = 8$ .

$$\gamma_{\eta}^{\mu} = \left[ 2\Gamma_{\eta\delta}^{\mu} u^{\delta} (u^0)^{-1} - \frac{q}{mu^0} F_{\eta}^{\mu} \right]_{y=0}, \quad (19)$$

$$U^{\mu} = \left[ \gamma_{\eta}^{\mu} u^{\eta} (u^0)^{-1} - \frac{q}{mu^0} F_{\eta}^{\mu} u^{\eta} (u^0)^{-1} \right]_{y=0}, \quad (20)$$

where the external force presents as  $f_{\nu}^{\mu} u^{\nu} (u^0)^{-1}$ , and the four-velocity for the circular orbits in the equatorial plane is  $u^{\mu} = u^0(1, 0, 0, \Omega)$  [28]. The integration of equation (18) for the  $t$  and  $\phi$  components gives us

$$\frac{d\xi^{\eta}}{dt} + \gamma_{\nu}^{\eta} \xi^{\nu} = \frac{q}{mu^0} \int f^{\eta} dt, \quad (21)$$

$$\frac{d^2 \xi^x}{dt^2} + \omega_x^2 \xi^x = \frac{q}{mu^0} \left( f^x - \gamma_{\eta}^x \int f^{\eta} dt \right), \quad (22)$$

$$\frac{d^2 \xi^y}{dt^2} + \omega_x^2 \xi^y = \frac{q}{mu^0} f^y. \quad (23)$$

where here  $\eta$  can be taken as  $t$  or  $\phi$ , and

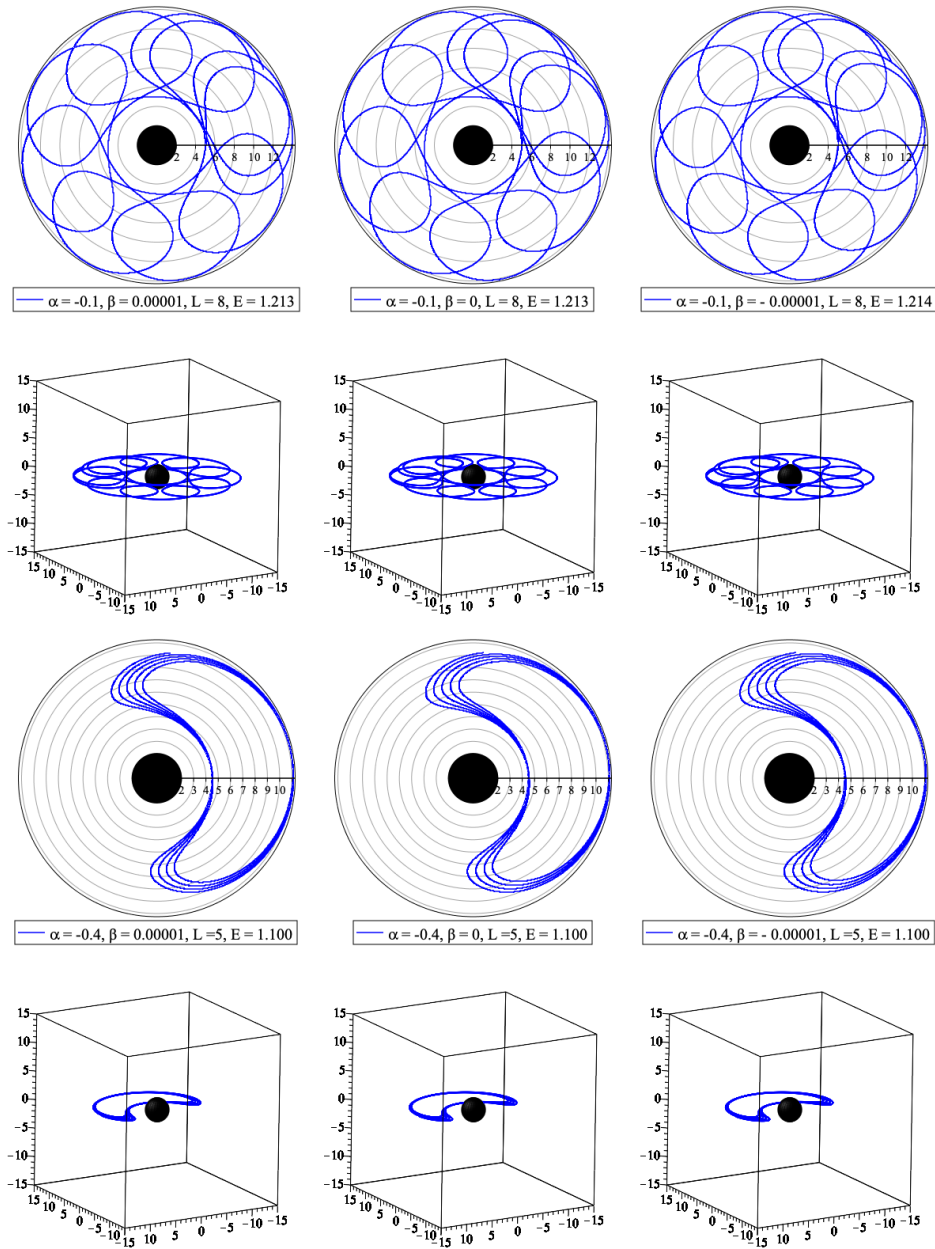


FIG. 3. Trajectories of particles for some choices of the parameters. In all plots  $Q > 0$  and  $\alpha < 0$ . In the first row, the initial radius is set to be  $r_0 = 5$ , and in the second one is  $r_0 = 4.5$ .

lyze the behavior of these frequencies (24).

$$\begin{aligned}\omega_x^2 &= \partial_x U^x - \gamma^x_\eta \gamma^\eta_x, \\ \omega_y^2 &= \partial_y U^y.\end{aligned}\quad (24)$$

This system of equations describes radial phase and vertical oscillations of the charged particle around the circular orbits [73]. The positive sign of the squared frequencies (24) determines the stability of circular orbits; otherwise, even a minimal perturbation can deviate substantially from the unperturbed orbit. In the absence of the external force, these equations describe the free radial phase and vertical oscillations of particles around the circular orbits. In what follows, we ana-

### A. Properties of epicyclic frequencies

The correspondence frequencies of the equation (24) in the background of a distorted, deformed compact object, explicitly are written in the appendix A. In this case, as equations (A1) and (A2) suggest, we can not write  $\omega_x$  and  $\omega_y$  as some coefficient of  $\Omega$ , like the standard procedure in Schwarzschild and Kerr space-times. However, this procedure is possible in this metric only when there is no magnetic field presented.

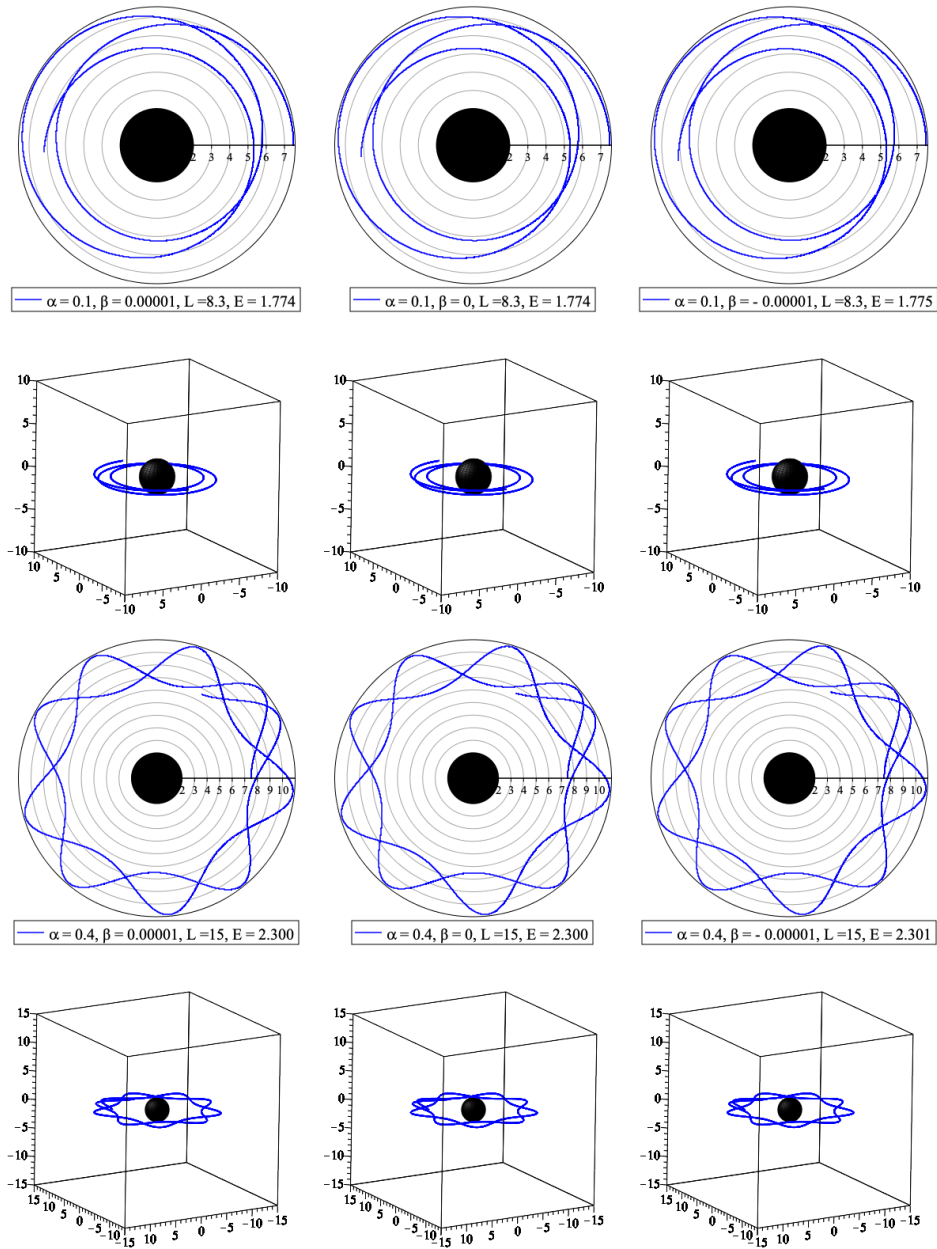


FIG. 4. Trajectories of particles for some choices of the parameters. In all plots  $Q < 0$  and  $\alpha > 0$ . In the plots, the initial radius is set to be  $r_0 = 7.5$ .

In Figure 5 and 6 we see the locations of maxima of these frequencies  $\omega_x$  and  $\omega_y$ . For any choice of parameters, the radial frequency's extrema must be located above the marginally stable orbit. The extrema are dependent on the choice of parameters for the vertical frequency, but these are always a monotonic function of distance  $x$ .

Figures 7 and 8 are depicted for the study of the existence and the stability of the timelike orbits with respect to vertical or radial oscillations. All the plots in Figure 7 are in the  $(x, \beta)$ -plane for two chosen values of the deformation parameter  $\alpha$  - one positive and one negative- and for different values of the magnetic parameter  $Q$ . While Figure 8 represents the

region of existence and stability in the  $(x, \alpha)$ -plane for two chosen values of the distortion parameter  $\beta$ , and for the same values for the magnetic parameter  $Q$  as in Figure 7.

Figure 9 is an extension of Figure 8 only for negative values of  $Q$  close to zero. On the three Figures 7-9, the red line and the blue line correspond to  $w_x^2 = 0$  and  $w_y^2 = 0$ , respectively. The dark-green region bounded by those two blue and red lines represents the area where both are positive  $w_x^2 > 0$  and  $w_y^2 > 0$ , which is the condition to have stability with respect to vertical and radial oscillations. Note that above the red line, where we have  $w_x^2 < 0$  and  $w_y^2 > 0$ , orbits are stable with respect to vertical oscillations but unstable to the radial

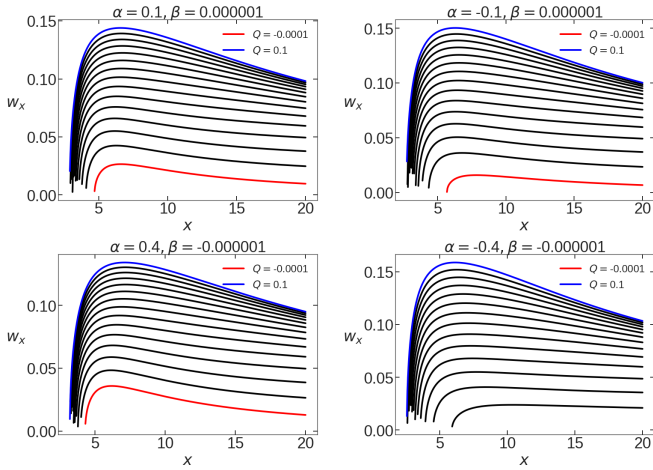


FIG. 5. The radial epicyclic frequency  $w_x$  is plotted with respect to  $x$  for four different pairs of  $(\alpha, \beta)$ . On each plot, different values of  $Q$  are used from  $Q = -0.0001$  to  $Q = 0.1$ . The blue curve corresponds to  $Q = 0.1$  and the red curve to  $Q = -0.0001$ . We can note for the pair  $(-0.4, -0.000001)$ , the red curve ( $Q = -0.0001$ ) is not appearing. This means that for these values of  $\alpha$  and  $\beta$ , the radial epicyclic frequency is not real.

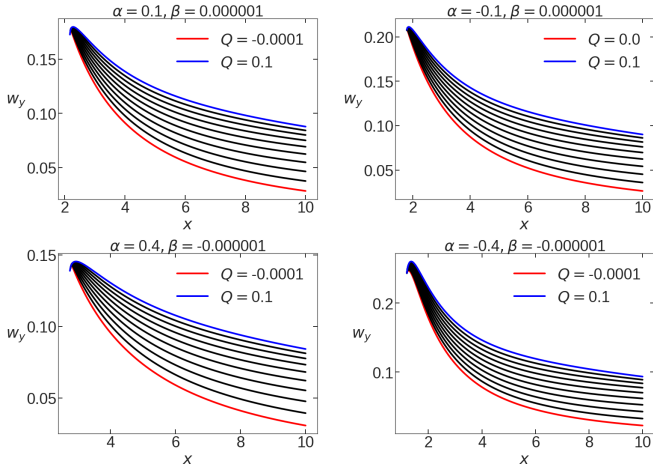


FIG. 6. The vertical epicyclic frequency  $w_y$  is plotted with respect to  $x$  for four different pairs of  $(\alpha, \beta)$ . On each plot, different values of  $Q$  are used from  $Q = -0.0001$  to  $Q = 0.1$ . The blue curve corresponds to  $Q = 0.1$  and the red curve to  $Q = -0.0001$ .

one. And on the contrary, below the blue line, where  $w_x^2 > 0$  and  $w_y^2 < 0$ , the orbits are stable with respect to radial oscillations and unstable with respect to the vertical one. We analyze these Figures by exploring the existence of the time-like circular orbit for different parameters. In fact, the region of existence is clearly affected by the three parameters. In the  $(x, \beta)$ - plane in Figure 10, we see that switching  $\alpha$  from negative to positive values tends to shrink the light-green region, on the contrary to an increase in  $\beta$ . The effect of the magnetic parameter is not monotonic; namely, by decreasing  $Q$  from positive to zero, the region is reduced in the vertical direction, but when  $Q$  becomes negative and still we continue to decrease it, the region extends again.

Let's focus now on the stability region (dark-green area). As for the existing area, all three parameters also have influence on the region of stability but with different strengths. We can note that switching  $\beta$  from negative to positive values makes the area of stability shrink (see Figure 8). The opposite effect is visible when switching  $\alpha$  from negative to positive (see Figure 10). However, the region of stability hardly changes with the parameter  $Q$ . It starts to shrink when  $Q$  decreases and continues by being pushed away from the central mass and then completely disappear for the negative values. This due to the fact that, on the  $(x, \beta)$ - plane, the blue curve comes up, and the red one comes down, so the dark-green region shrinks, and at the end does not exist anymore. For larger negative values, a branch from above comes back in the physical range but keeps staying below the blue curve. On the  $(x, \alpha)$ - plane, this is due to the fact that the red curve goes up and then goes out from the physical range. This effect can be seen by combining Figures 8 and 9. This situation is mainly like what is happening for negatives values of  $Q$ . A small area remains for values of the magnetic parameter close to zero  $Q = -0.01$ . In this case, it means there is no stable orbit in any direction in the chosen physical range.

In Figures 10 and 11, different relations between the frequencies have been plotted. Similar to Figures 7 and 8 the red and the blue curves are representing  $w_x^2 = 0$  and  $w_y^2 = 0$ , respectively. We add to this picture more information that helps to analyze the order of the different epicyclic frequencies  $w_x^2$ ,  $w_y^2$  and  $\Omega^2$  easier. The orange line shows  $w_y^2 = \Omega^2$ , which leads to the hatched line region  $w_y^2 > \Omega^2$ . Also,  $w_x^2 = \Omega^2$  corresponds to the pink line related to the dark-green area where  $w_x^2 > \Omega^2$ . Furthermore,  $w_x^2 = w_y^2$  is shown by the yellow line. The corresponding region  $w_x^2 > w_y^2$  is presented in the hatched dotted line. By analyzing both Figures together, we can order the frequencies as a function of the magnetic parameter  $Q$ . We see that for  $Q \geq 0$ , the order's behavior will depend on two crossing points. One when the orange line crossed the red line and another when the orange, pink and yellow all are crossing.

For small values of  $\beta$ , the order is pretty steady (see plots with  $Q \geq 0$  on the left in Figure 11). However, by increasing  $\beta$ , the crossing points appear, then the behaviour of ordering becomes more complicated (see plots with  $Q \geq 0$  on the left in Figure 10). For instance, using the second plot of the first raw of Figure 10 in the stable region; namely, between the red and blue lines, the frequencies are ordered as follow:

- (i) Inside the hatched region (above the orange line) where  $\beta$  is close to zero, and  $\alpha$  is positive or negative:
  - (a) from the red line to the pink one:  $w_x^2 < \Omega^2 < w_y^2$ ,
  - (b) from the pink line to the yellow one:  $\Omega^2 < w_x^2 < w_y^2$ ,
  - (c) above the yellow line:  $\Omega^2 < w_y^2 < w_x^2$ .
- (ii) Outside the hatched region (below the orange line), where  $\beta$  has larger negative values, the order of the frequencies is different:
  - (a) from the red line to the yellow one:  $w_x^2 < w_y^2 < \Omega^2$ ,



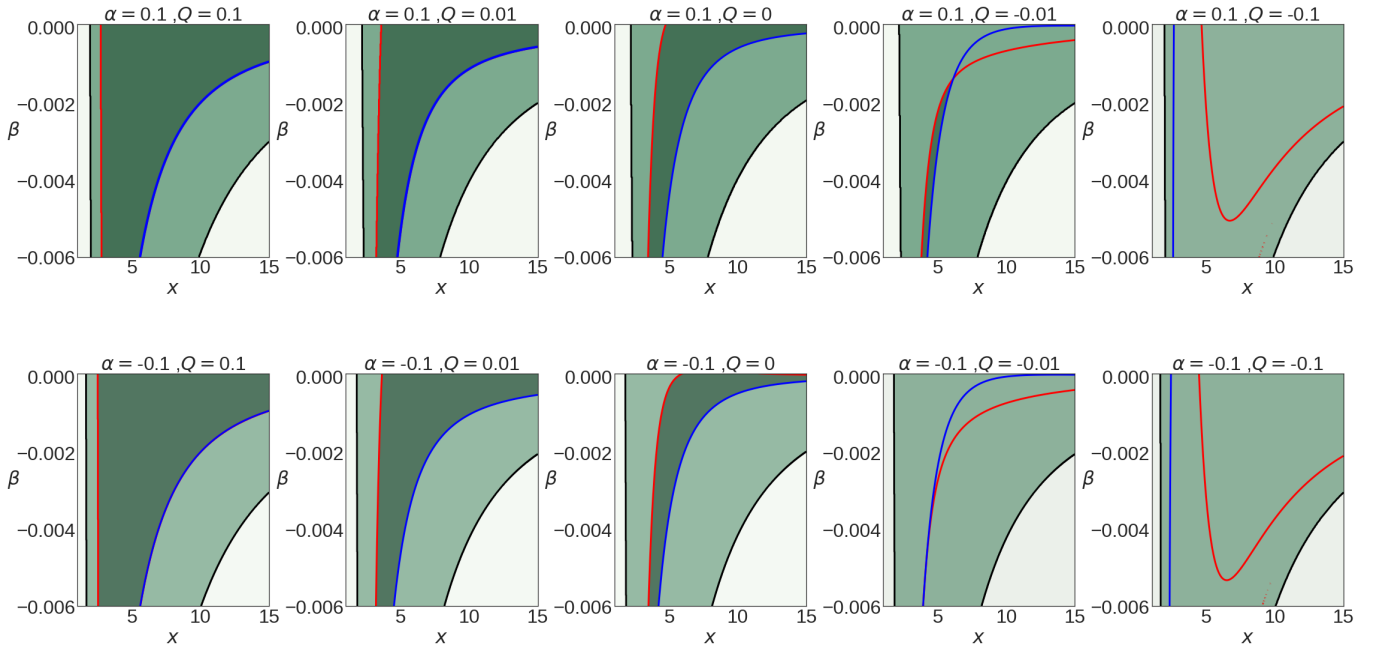


FIG. 7. Stability of the timelike circular orbits of a charged particle in the  $(x, \beta)$ -plane. Timelike circular orbits can exist in the green light area. The blue curve represents  $w_y^2 = 0$  and the red one  $w_x^2 = 0$ . Timelike orbits are stable with respect to vertical and radial perturbations in the region where  $w_x^2 > 0$  and  $w_y^2 > 0$ . This area is depicted by the green-gray region, which combined the conditions of existence and the condition of stability,  $w_x^2 > 0$  and  $w_y^2 > 0$ . The analysis is done for two positive values of  $Q$ , two negatives values of  $Q$ , and the unmagnetized case  $Q = 0$ .

- (b) from the yellow line to the pink one:  $w_y^2 < w_x^2 < \Omega^2$ ,
- (c) and above the pink line:  $w_y^2 < \Omega^2 < w_x^2$ .

About negative values of  $Q$ , the order's distribution is different; however, the analysis is simple because the region of stability is strongly reduced. In this Figure, the only stable region appears for the positive value of  $\alpha$  and the case  $Q = -0.01$  (the fourth plot of the top line in Figure 11). In this small stable region (dark-green region in the corresponding plot in Figure 8) the order is as follow:

- (i) from the red to the yellow line (small extended vertically region):  $w_x^2 < w_y^2 < \Omega^2$ ,
- (ii) from the yellow line to the blue one:  $w_y^2 < w_x^2 < \Omega^2$ .

To sum up, increasing  $Q$  makes the region of specific order larger and creates new regions where one can find different orders for the frequencies.

## V. QPO MODELS

A class of models, so-called orbital models, assume a relation between the QPO frequencies and the frequencies related to motion of accreted matter orbiting in the vicinity of a compact object. These models focus on hot-spot or disc-oscillation to describe QPOs. However, the existing QPO models are incomplete tasks. Since the oscillations predicted

by these models are usually not seen in the same way in the MHD simulations. Furthermore, none of these models has a good match, especially with the full QPOs amplitudes and the visibility on the source spectral data, in the LMXBs.

Among these various models we consider the group of QPO models considered in [74] and examine them in this set-up. For a detailed discussion on these models see also [48, 75–77]. In this section, we begin by explaining the main features of each model briefly. As we see in the following, their prescriptions rely on the formulae for epicyclic frequencies of a particle motion [74] which are shared the primary motivation with some cases for example models based on the dynamic of fluid [53]. In fact, in a given model, the predicted QPOs can be expressed in the test particle motion with reasonable accuracy even for the consideration of discoseismic modes. In the following, the two kinematic models are RP and TD, and the resonant models are WD, Ep, Kp, RP1 and RP2. In fact, they consider different possibilities in the combination of disc-oscillation modes. In brief, in the concept of resonance hypothesis [42], the two modes in resonance should have eigenfrequencies equal to the radial epicyclic frequency and to the vertical epicyclic frequency or to the Keplerian frequency [74, 75, 78]. Besides, models based on the parametric resonance identify the two observed frequencies of  $(\nu_U, \nu_L)$  directly with the eigenfrequencies of a resonance. On the other hand, models based on the forced resonance allows to observe combinational frequencies of the modes. Both parametric and forced resonance models provide precise predictions about the values of observed frequencies considering spin and mass of the observed object in particular in the black hole sources.

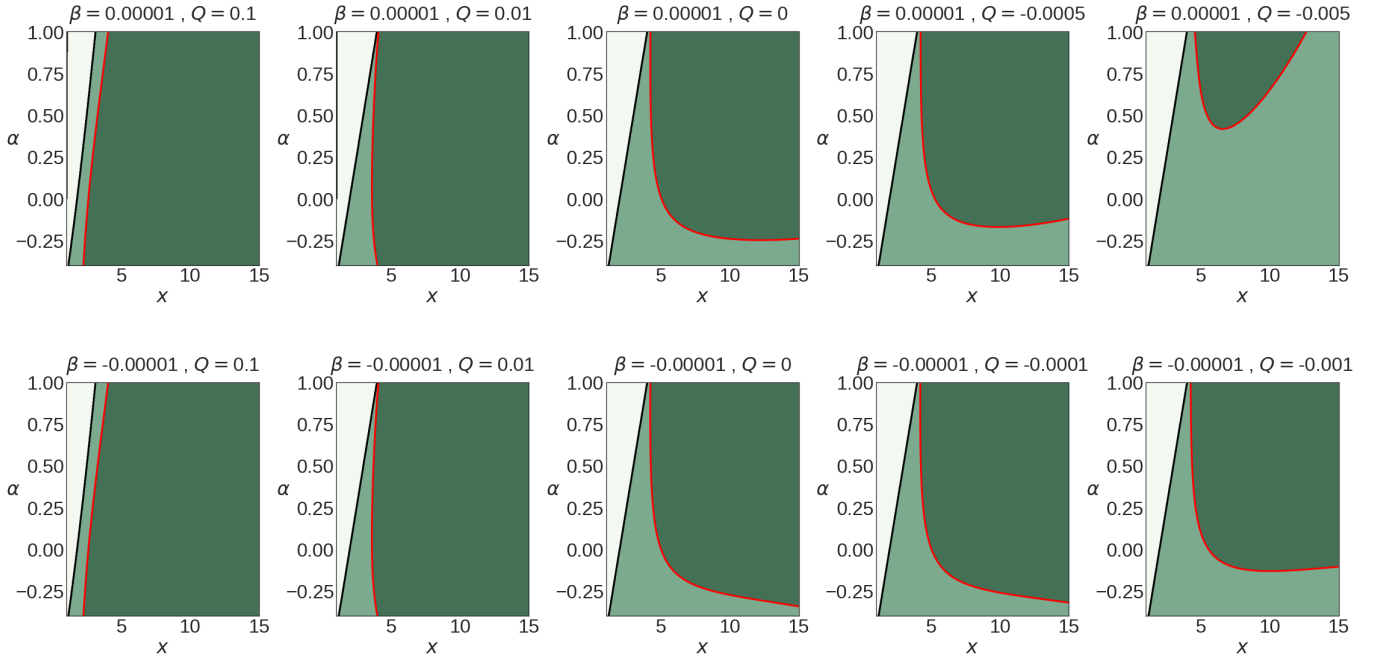


FIG. 8. Stability of the timelike circular orbits in the  $(x, \beta)$ -plane. Timelike circular orbits exist in the green light area. The blue curve represents  $w_y^2 = 0$  and the red one  $w_x^2 = 0$ . Timelike orbits are stable with respect to vertical and radial perturbations in the region where  $w_x^2 > 0$  and  $w_y^2 > 0$ . The analysis has done for two positive values of  $Q$ , two negatives values of  $Q$ , also for the unmagnetized case  $Q = 0$ .

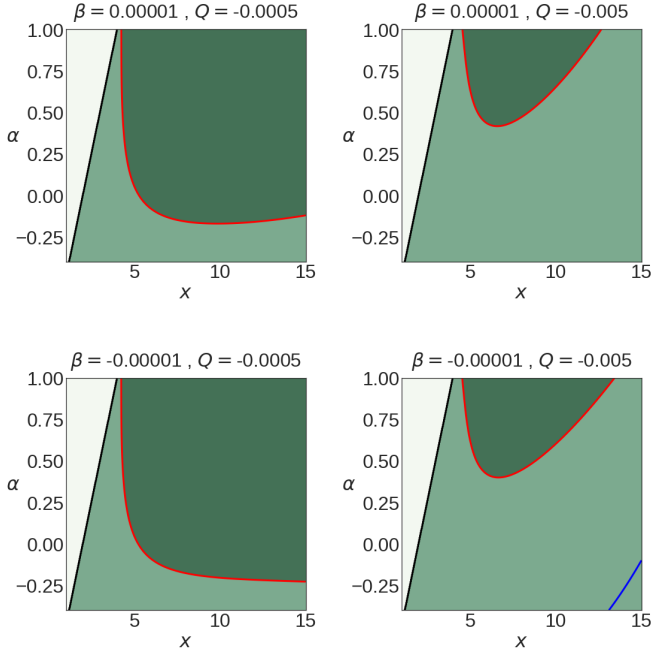


FIG. 9. Stability of the timelike circular orbits in the  $(x, \alpha)$ -plane. We zoomed in for the small negative values of  $Q$ . These two columns can be inserted between the 3rd and 4th columns of Figure 8. The description of the regions and curves are the same as Figure 8.

### A. RPM

The Relativistic Precession Model (RPM) is one of the first attempts to model QPOs, proposed in [26, 79]. In RPM the upper frequency is defined as the Keplerian frequency  $\nu_U = \Omega$  and the lower frequency is defined as the periastron frequency i.e.  $\nu_p := \nu_L = \Omega - \nu_x$ . Their correlations are obtained by varying the radius of the associated circular orbit. Within this framework, it is usually assumed that the variable component of the observed X-ray arises from the motion of “hot-spots” or biting inside the accretion disc on a slightly eccentric orbit. Therefore, due to the relativistic effects, the observed radiation is supposed to be periodically modulated. In this model, frequencies predicted are scaled as  $1/M$  for a fixed spin value; therefore, the expected frequency ratio is mass independent. As a weakness of this model is the lack of a generic explanation for the observed 3 : 2 frequency ratio.

### B. TDM

Another kinematic model is the Tidal Disruption Model (TDM) presented in [80, 81]. This follows also very similar approach as the RPM. In this model, the QPOs are assumed as a result of tidal disruption of large accreting inhomogeneities. In other words, when blobs orbiting the central compact object can be stretched by tidal forces forming the ring-section. However, in this case also the frequency ratio is not reliably constrained. In TDM the frequencies are identified with the frequencies of the orbital motion; namely, the upper frequency is defined as  $\nu_U = \Omega + \omega_x$  and the lower frequency is defined

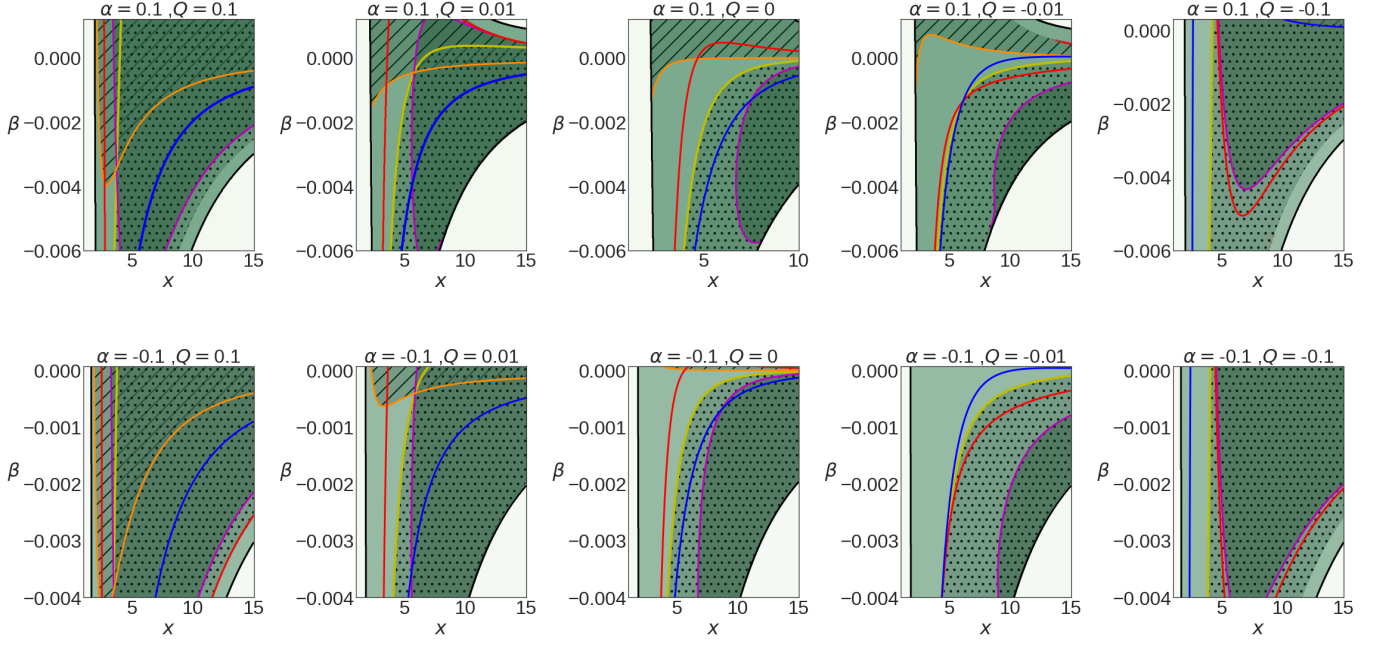


FIG. 10. Order of the different epicyclic frequencies in the  $(x, \beta)$ -plane. Timelike circular orbits can exist in the green light area. The blue curve represents  $w_y^2 = 0$  and the red one  $w_x^2 = 0$ . The pink, orange and yellow depicts  $w_x^2 = \Omega^2$ ,  $w_y^2 = \Omega^2$  and  $w_x^2 = w_y^2$ , respectively. The green-gray area shows the region where  $w_x^2 > \Omega^2$ . The hatched line region represents the area where  $w_y^2 > \Omega^2$ . Also, the hatched dotted area is where  $w_x^2 > w_y^2$ . The analysis has done for different values of  $Q$ . Besides, two different values of the deformation parameter  $\alpha$  has been tested.

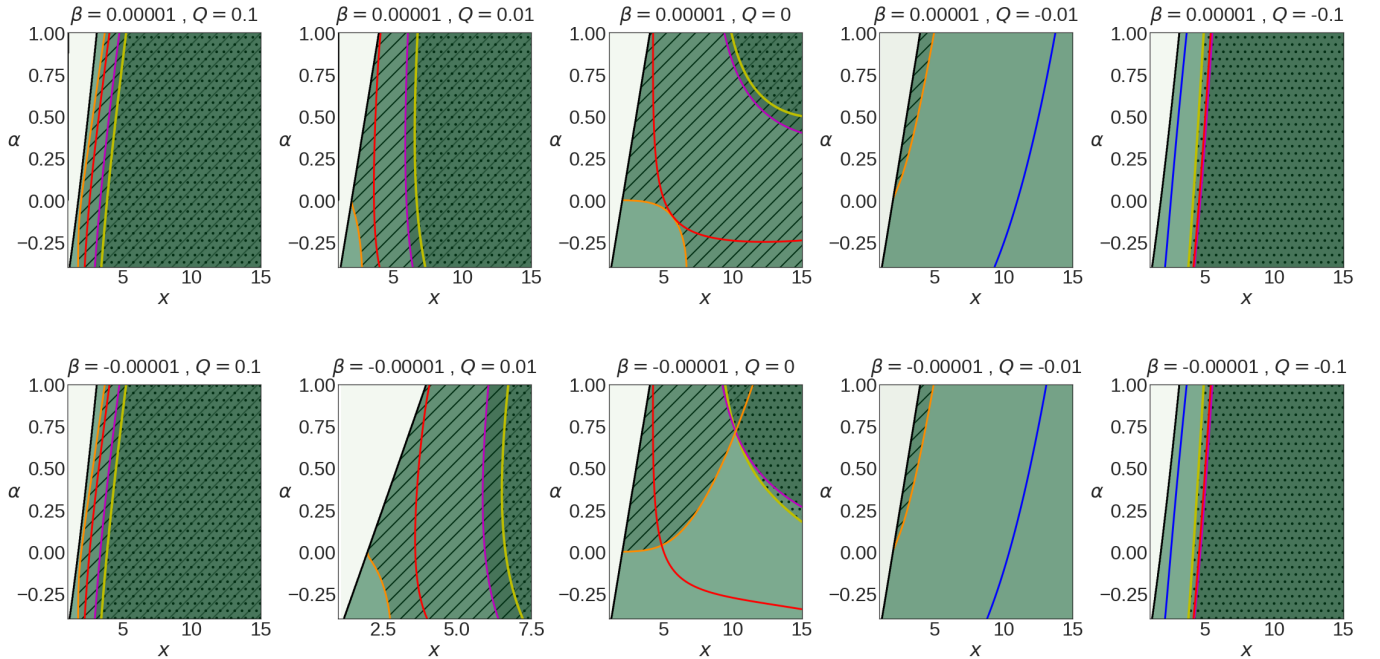


FIG. 11. Order of the different epicyclic frequencies in the  $(x, \alpha)$ -plane. Timelike circular orbits exist in the green light area. The blue curve represents  $w_y^2 = 0$  and the red one  $w_x^2 = 0$ . The pink, orange and yellow depicts  $w_x^2 = \Omega^2$ ,  $w_y^2 = \Omega^2$  and  $w_x^2 = w_y^2$ , respectively. The green-gray area shows the region where  $w_x^2 > \Omega^2$ . The hatched line region represents the area where  $w_y^2 > \Omega^2$ . Finally, the hatched dotted area is where  $w_x^2 > w_y^2$ . The analysis has done with the focus on the different signs of  $Q$ . In addition, two different values of the deformation parameter  $\beta$  has been tested.

| Model | $\nu_U$              | $\nu_L$               |
|-------|----------------------|-----------------------|
| RP    | $\Omega$             | $\Omega - \omega_x$   |
| Kp    | $\Omega$             | $\omega_x$            |
| Ep    | $\omega_y$           | $\omega_x$            |
| TD    | $\Omega + \omega_x$  | $\Omega$              |
| WD    | $2\Omega - \omega_x$ | $2\Omega - 2\omega_x$ |
| RP1   | $\omega_y$           | $\Omega - \omega_x$   |
| RP2   | $2\Omega - \omega_y$ | $\Omega - \omega_x$   |

TABLE I. Frequency relations corresponding to individual QPO models

as  $\nu_L = \Omega$ .

### C. WDM

The Warped disc Model (WDM) introduced in [82], which is related to non-axisymmetric modes in a warped accretion disc. In WDM the upper frequency is defined as  $\nu_U = 2\Omega - \omega_x$  and the lower frequency is  $\nu_L = 2\Omega - 2\omega_x$ . In more realistic versions of this model, the higher harmonic oscillations are also considered up to the third order, then frequencies like  $3\Omega - \omega_x$  possible to consider. On the contrary with two last models, the ratio of the frequencies is crucial for the model. However, this model suffers from the fact that it considers a somehow exotic disc geometry that causes a doubling of the observed lower QPO frequency.

### D. EpM-KpM

The Epicyclic resonance Model (EpM) [75] is the simplest variant. It is about considering radial and vertical epicyclic oscillations and relates them to the resonance of axisymmetric disc-oscillation modes. The Keplerian resonance Model (KpM) considers a resonance between the orbital Keplerian and the radial epicyclic oscillations. In EpM the upper frequency is defined as  $\nu_U = \omega_y$  and the lower frequency is  $\nu_L = \omega_x$ . In KpM the upper frequency is defined as  $\nu_U = \Omega$  and the lower frequency is  $\nu_L = \omega_x$ .

### E. RP1M-RP2M

The RP1 model by Bursa in 2005 and the RP2 model [30], both consider different combinations of non-axisymmetric disc-oscillation modes. In RP1M the upper frequency is defined as the Keplerian frequency  $\nu_U = \omega_y$ , and the lower frequency is  $\nu_L = \Omega - \omega_x$ . In RP2M the upper frequency is defined as  $\nu_U = 2\Omega - \omega_y$  and the lower frequency is  $\nu_L = \Omega - \omega_x$ . In the case of slow rotation, their outcome frequencies of oscillation modes are almost coincide with the frequencies predicted by the RPM.

The behaviour of these models is illustrated in Figures 12 and 13. In these Figures, the radius of the 3 : 2 frequencies for the different models (WD, TD, RP, Ep, Kp, RP1, RP2) is

plotted, with respect to the deformation parameter  $\alpha$ , and for two chosen values of the distortion parameter  $\beta$ .

This radius depends on all parameters  $\alpha$ ,  $\beta$ , and  $Q$ . Nevertheless, on both Figures, Our primary focus is on the impact of the parameter  $Q$ . As it is seen in Section IV A where we discussed about the existence and stability of the timelike orbits, only small negative values of  $Q$  allow having stability with respect to both vertical and radial oscillations.

From the Figures 12 and 13 we can see that for negatives values of  $Q$ , two radii can satisfy the 3 : 2 ratio. This situation also happens for all models. Besides, increasing  $Q$  tends to move the maximum of the curve to the right. Thus, increasing  $Q$  allows choosing larger interval for  $\alpha$  where the radius of the 3 : 2 ratio exists. Furthermore, increasing the magnetic parameter causes to push this radius closer to the central object. About the different models, we can see that the 3 : 2 ratio of the RPM, RP1M, and RP2M appears at the radii similar to each other. As mentioned in the VE, this is what we expected for a slow rotating set-up. The same effect is seen for the EpM and KpM. However, models seems to deviate from each other in the case of  $Q < 0$  in the upper part of the curves. Furthermore, Figure 13 shows that in general, the behavior of the negative  $\beta$  is very similar to the positive  $\beta$  which is discussed earlier. However, slight differences occur on the curves' upper branch for the negative value of  $Q$ , where in this case, the KpM and EpM diverge from each other. The same is true for RP1M, RP2M, and RPM.

This is worth mentioning that in this deformed and distorted background, with different combinations of parameters  $\alpha$ ,  $\beta$  and  $Q$ , it is possible to have other ratios which can be relevant in other observed data like in other frequencies observed in the Microquasar GRS 1915 + 105, see for example [83]. In addition, the models that associate the variabilities in HF QPQ with discoseismic oscillation modes of the accretion disc, determined that even a weak magnetic field can strongly affect the g-modes [84, 85]. Therefore, it also seems reasonable to study the impact of the deformation parameter on these modes. A preliminary investigation reveals that even a slight increase in  $\alpha$  changes the corresponding area of the g-mode, manifestly. However, this critical result needs further consideration and can be a future work.

## VI. COMPARISON WITH THE OBSERVATIONS

The results of fitting the charged particle oscillation frequencies to the observed frequencies of three microquasars XTE 1550–564, GRS 1915+105, and GRO 1655–40 [86, 87] listed in Table II, are presented in Figures 14 and 15. Indeed, significant spin is expected in astrophysical black holes at all scales, therefore it is important to develop the model that encodes spin as well, which is in progress. Of course, considering rotation like magnetic field likely to modify the radial profiles of frequencies. Nevertheless, this preliminary results show the fitting can be done even for the fast-rotating microquasar GRS 1915 + 105.

The observed values of the HF QPO frequencies for this three sources show  $\nu_U : \nu_L = 3 : 2$  ratio [86, 87]. In Figure

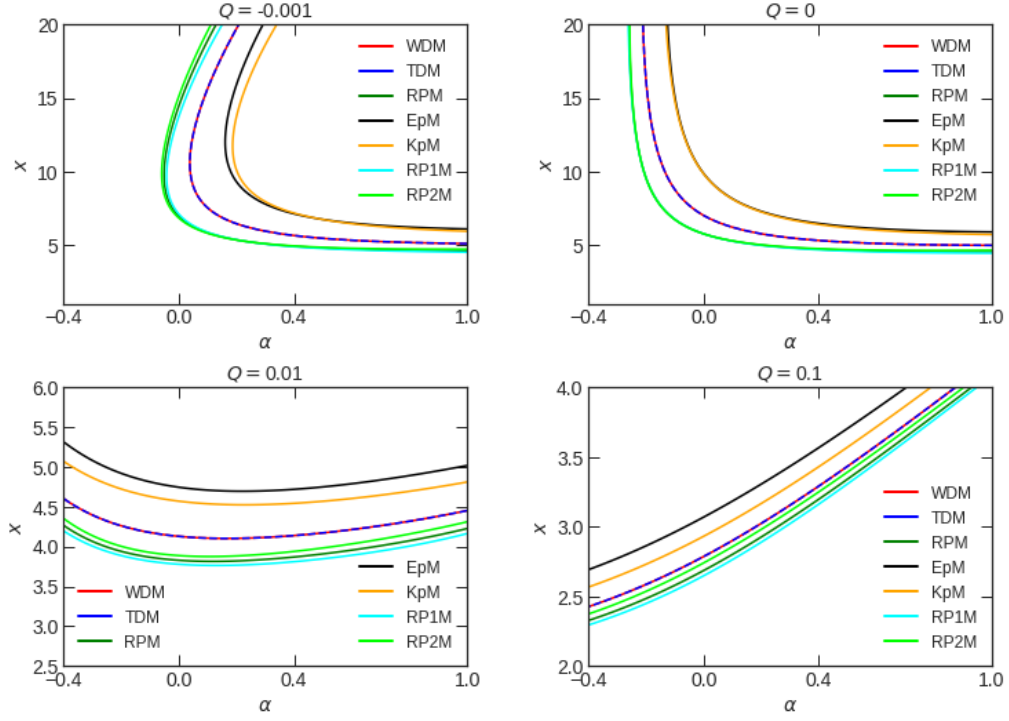


FIG. 12. The radii of the 3 : 2 frequency ratio for different models. The radius is the function of the  $\alpha$  parameter for different values of the magnetic term  $Q$ . On all the plots,  $\beta = 0.000001$ .

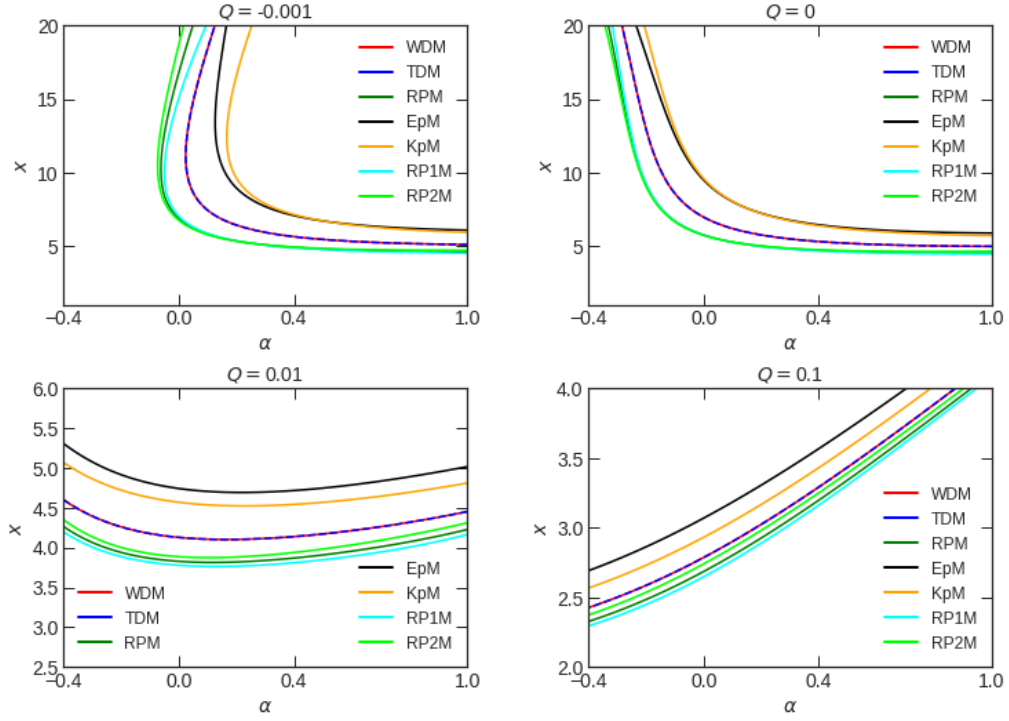


FIG. 13. The radii of the 3:2 frequency ratio for different models. The radius is the function of the  $\alpha$  parameter for different values of the magnetic term  $Q$ . On all the plots,  $\beta = -0.000005$ .

| Source              | GRO 1655 – 40 | XTE 1550 – 564 | GRS 1915 + 105 |
|---------------------|---------------|----------------|----------------|
| $\nu_U$             | 447 – 453     | 273 – 279      | 165 – 171      |
| $\nu_L$             | 295 – 305     | 179 – 189      | 108 – 118      |
| $\frac{M}{M_\odot}$ | 6.03 – 6.57   | 8.5 – 9.7      | 9.6 – 18.4     |
| $a$                 | 0.65 – 0.75   | 0.29 – 0.52    | 0.98 – 1       |

TABLE II. Observed HF QPO data for the three micro-quasars, independent of the HF QPO measurement, and based on the spectral continuum fitting.

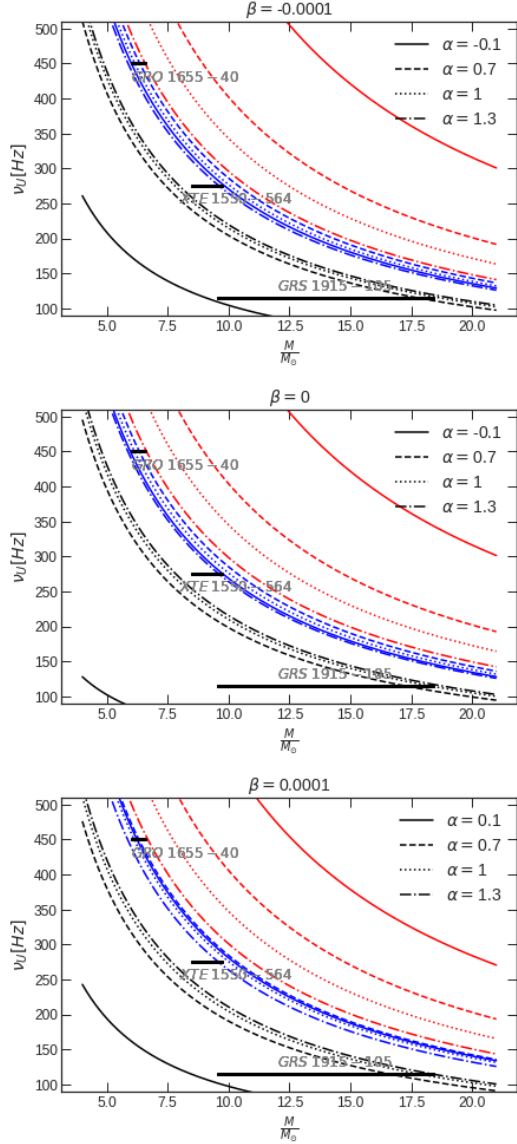


FIG. 14. The upper oscillation frequency  $\nu_U$  at the resonance radius 3 : 2 is presented for various combinations of the studied parameters for the EP model. The magnetic parameter vary with the color's lines. The black lines depict  $Q = 0$  (unmagnetized case). The blue lines show  $Q = 0.01$  and the red lines present  $Q = 0.1$ . The upper frequency is compared to the mass-limits obtained from observations of three mentioned microquasars.

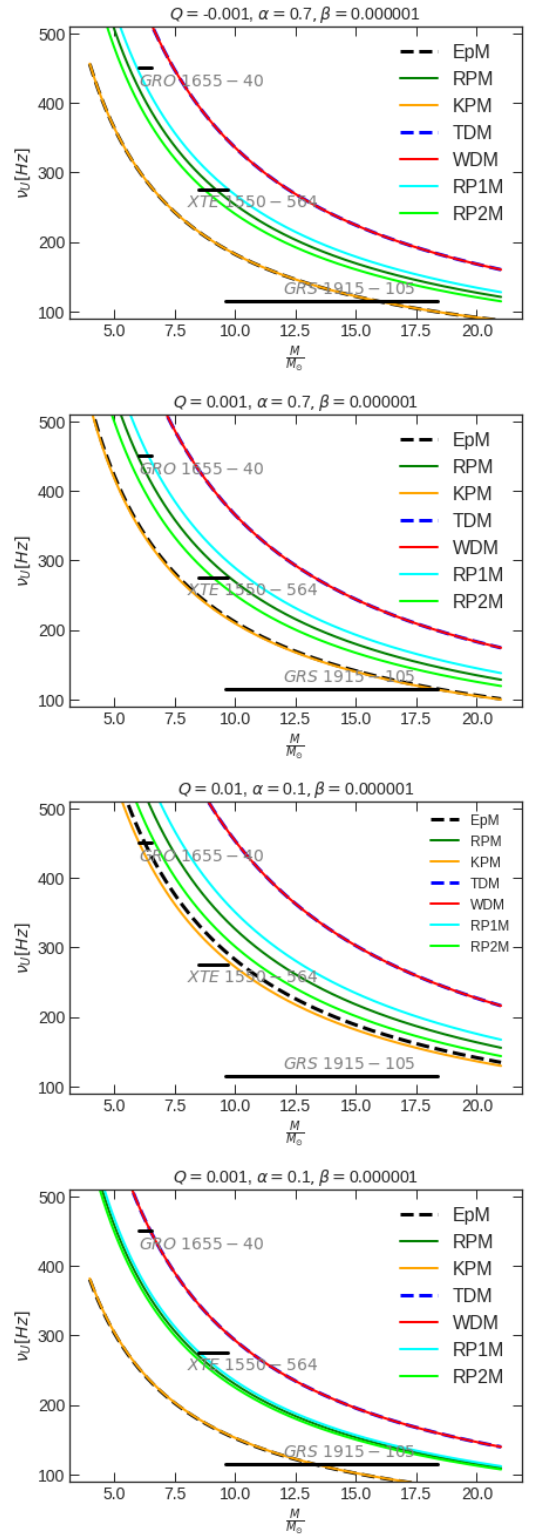


FIG. 15. The upper oscillation frequencies for the models presented in the Table I are compared to the mass-limits obtained from observations of three microquasars for various set of parameters.

14 we fixed the resonance model EP and try to find the best fitting by exercising different parameters of the model; the deformation  $\alpha$ , the distortion  $\beta$  and the magnetic parameter  $Q$ .

In Figure 14 each plot corresponds to different values of the distorted parameter  $\beta$ , and the line styles present various deformation parameter  $\alpha$ . The different colors also related to different magnetic parameters. Interestingly, a direct inspection of the various combinations of the parameters shows the crossing with the data lines. While the fitting totally depends on the combination of all parameters, but in general, we can expect to have a better fitting for choosing a larger  $\alpha$  in the combination.

In Figure 15 we have analyzed the different models presented in the last section (see the Table I). Especially, as we have some freedom in choosing the model's parameters, we have decided on ones that minimize computational time and numerical errors and fit the best with data considering Figures 12 and 13.

In fact, we note that although different sets of parameters can fit the data, even for the fast-rotating source as GRS 1915 + 105 and GRO 1655 – 40; nonetheless, we focus on the fitting to the relatively slowly rotating XTE 1550 – 564 source which is more compatible with our set-up. As Figure 15 suggests, for chosen parameters  $Q$ ,  $\alpha$ , and  $\beta$ ; the best fit almost corresponds to RP2M, RPM, and RP1M in low spin cases. KpM and EpM seem to be in favour of the high spin sources. It is worth comparing this result with the behaviour of these models in Kerr spacetime [74]. In general, it appears that a non-zero magnetic field facilitates the fitting procedure. As a result, we find that WDM and TDM almost have similar behaviour. The same is true for EpM and KpM, while RP1M, RP2M, and RPM may deviate from each other depending on the magnetic field and deformation parameter  $\alpha$ . These results are almost compatible with the result in Kerr spacetime, where spin plays a similar role to  $\alpha$  [74]. More precisely, by increasing  $\alpha$  the deviation between RP's models increases. In this way, studying these three models and the deviations from each other may play an important role to recognize the oblateness of the source from observational data. However, a deeper analysis shows that we can note that almost for  $\alpha \in [0.1, 0.9]$  one can have a better fitting to observations.

Further analysis reveals that the curves take their minimum at different radii depending on the choice of parameters. We see that in all cases, almost the positive and negative values of  $\beta$  take their maximum at the same radii; however, further investigation indicates that these radii are smaller for negative values of this parameter  $\beta$ . Also, the maximums in all curves in the desirable domain depend on the ratio; for example, we see that as this ratio becomes larger, maximum of a curve happens in the smaller radius. This means that the resonance is not monotonic after some distance from the central object, and it depends on the combination of parameters in this set-up.

## VII. SUMMARY AND CONCLUSION

In this paper, we studied the dynamics of test charged particles in the presence of an asymptotic uniform magnetic field.

Further, we have examined different QPO models considered in [74] in the vicinity of a deformed compact object up to the quadrupole. This space-time is a generalization of the q-metric which is static and axisymmetric. It contains two distortion parameter  $\beta$  and deformation parameter  $\alpha$  which briefly explained in Section II. These two parameters alter the motion and epicyclic frequencies of charged particles moving in this background. However, our main focus was to analyze the influence of magnetic parameters on this set-up. In this manner, the results exhibit a substantial deviation from the nonmagnetic case. It has shown that a regular orbit for some combinations of metric parameters turn to behave chaotically with a magnetic field. Further inspection revealed that magnetic parameter also brings a profound impact on the dynamics and on the radial and vertical frequencies around a stable equatorial orbit.

Additionally, we have shown that the resonant phenomena of the radial and vertical oscillations at their frequency ratio 3 : 2, depending on chosen parameters of the model, can be well fitted to the HF QPOs observed in the microquasars GRS 1915 + 105, XTE 1550 – 564, GRO 1655 – 40. In fact, this model may open up a variety of exciting applications in general relativity and astrophysics.

Additionally, it is possible from observational data or other analytic set-ups to assign some restrictions on the parameters in this metric. Moreover, the next step of this work would be to consider models based on the dynamics of fluid in this set-up. This is also possible to explore more about the observational data by considering different inputs in this model, which is the subject of the following work. For example, considering rotation definitely helps to model a more realistic complex system of astronomical objects, or a key direction for future work may be adding the strong magnetic field, which also influences the metric itself.

## Appendix A: Epicyclic frequencies in the uniform magnetic field

The following relations give epicyclic frequencies of particles' circular motion in the background of a distorted, deformed compact object immersed in a uniform magnetic field. The squared vertical frequency is given by

$$w_y^2 = e^{-2\tilde{\gamma}} \left( \frac{x^2 - 1}{x^2} \right)^{-\alpha(2+\alpha)} \left[ \Omega^2 \frac{x f_1(x, \beta) + S}{S} + (1 + f_1(x, \beta)) \Omega \omega_B \right], \quad (\text{A1})$$

And the radial one is given by

$$w_x^2 = \frac{\Omega^2 e^{-2\tilde{\gamma}} (1 - 1/x^2)^{-\alpha(2+\alpha)}}{x(1 - x^2)} \left[ g_1(x, \beta, \alpha) \frac{x - S}{S} + g_2(x, \beta, \alpha) \right] + \frac{e^{-2\tilde{\gamma}} (1 - 1/x^2)^{-\alpha(2+\alpha)}}{x(1 - x^2)} \left[ -\omega_B^2 x(S - x)^2 + \Omega \omega_B g_2(x, \beta, \alpha) \right], \quad (\text{A2})$$

where

## ACKNOWLEDGEMENTS

$$S = 1 + \alpha + \beta x - \beta x^3, \quad (\text{A3})$$

$$f_1(x, \beta) = \beta(-1 + 3x^2), \quad (\text{A4})$$

$$g_1(x, \beta, \alpha) = 2\alpha^3 + \alpha^2 \left( 6 - 2\beta x(-1 + x^2) \right) + \quad (\text{A5})$$

$$2\alpha \left( 2 + x \left( x + \beta(-1 + x^2) \left( -4 + \beta x(-1 + x^2) \right) \right) \right) +$$

$$x \left( 2x - \beta(-1 + x^2) \left( 5 + x \left( -x + 2\beta(-1 + x^2) \left( -3 + \beta x(-1 + x^2) \right) \right) \right) \right),$$

$$g_2(x, \beta, \alpha) = 2\alpha^3 - 4x \left( 1 + \alpha + (-1 + \beta)x - \beta x^3 \right)^2 \quad (\text{A6})$$

$$- 2\alpha^2 \left( -3 + x - \beta x + \beta x^3 \right)$$

$$+ 2\alpha \left( 2 + x \left( -2 + \beta(-1 + x^2) \left( -4 + \beta x(-1 + x^2) \right) \right) \right) - x \left( -1 + x^2 \right)$$

$$\times \left( -1 + \beta \left( 5 + x \left( -4 - 3x + 2\beta(-1 + x^2) \left( -3 + x - \beta x + \beta x^3 \right) \right) \right) \right).$$

The authors are grateful to Prof. Stuchlík and Dr. Kolos for a fruitful discussion and the anonymous referee for valuable comments that promoted the work. S.F. thanks the Cluster of Excellence EXC-2123 Quantum Frontiers - 390837967 and the research training group GRK 1620 "Models of Gravitational and the research training group GRK 1620 "Models of Gravity", founded by the German Research Foundation (DFG). A.T. thanks the research training group GRK 1620 "Models of Gravity", funded by DFG.

- 
- [1] Steven A. Balbus and John F. Hawley. A Powerful Local Shear Instability in Weakly Magnetized Disks. I. Linear Analysis. *Astrophys. J.*, 376:214, July 1991.
- [2] Claudio Cremaschini and Zdeněk Stuchlík. Magnetic loop generation by collisionless gravitationally bound plasmas in axisymmetric tori. *Phys. Rev. E*, 87(4):043113, April 2013.
- [3] C. Cremaschini, M. Tessarotto, and J. C. Miller. Absolute Stability of Axisymmetric Perturbations in Strongly Magnetized Collisionless Axisymmetric Accretion Disk Plasmas. *Phys. Rev. Lett.*, 108(10):101101, March 2012.
- [4] Claudio Cremaschini, Zdeněk Stuchlík, and Massimo Tessarotto. Kinetic theory of quasi-stationary collisionless axisymmetric plasmas in the presence of strong rotation phenomena. *Physics of Plasmas*, 20(5):052905, May 2013.
- [5] Robert M. Wald. Black hole in a uniform magnetic field. *Phys. Rev. D*, 10(6):1680–1685, September 1974.
- [6] Martin Kološ, Zdeněk Stuchlík, and Arman Tursunov. Quasi-harmonic oscillatory motion of charged particles around a Schwarzschild black hole immersed in a uniform magnetic field. *Classical and Quantum Gravity*, 32(16):165009, August 2015.
- [7] Bharat Ratra. Cosmological “Seed” Magnetic Field from Inflation. *ApJ*, 391:L1, May 1992.
- [8] D. Grasso and H. R. Rubinstein. Magnetic fields in the early Universe. *Phys. Rep.*, 348(3):163–266, July 2001.
- [9] Andrii Neronov and Ievgen Vovk. Evidence for Strong Extragalactic Magnetic Fields from Fermi Observations of TeV Blazars. *Science*, 328(5974):73, April 2010.
- [10] Rajeev Kumar Jain and Martin S. Sloth. Consistency relation for cosmic magnetic fields. *Phys. Rev. D*, 86(12):123528, December 2012.
- [11] Ruth Durrer and Andrii Neronov. Cosmological magnetic fields: their generation, evolution and observation. *Astron Astroph.*, 21:62, June 2013.
- [12] Jiří Kovář, Petr Slaný, Claudio Cremaschini, Zdeněk Stuchlík, Vladimír Karas, and Audrey Trova. Electrically charged matter in rigid rotation around magnetized black hole. *Phys. Rev. D*, 90(4):044029, August 2014.
- [13] Zdeněk Stuchlík and Martin Kološ. Acceleration of the charged particles due to chaotic scattering in the combined black hole gravitational field and asymptotically uniform magnetic field. *European Physical Journal C*, 76:32, January 2016.
- [14] Jiří Kovář, Zdeněk Stuchlík, and Vladimír Karas. Off-equatorial orbits in strong gravitational fields near compact objects. *Classical and Quantum Gravity*, 25(9):095011, May 2008.
- [15] O. Kopáček, V. Karas, J. Kovář, and Z. Stuchlík. Transition from Regular to Chaotic Circulation in Magnetized Coroneae near Compact Objects. *Astrophys. J.*, 722(2):1240–1259, October 2010.
- [16] J. Kovář, O. Kopáček, V. Karas, and Z. Stuchlík. Off-equatorial orbits in strong gravitational fields near compact objects—II: halo motion around magnetic compact stars and magnetized black holes. *Classical and Quantum Gravity*, 27(13):135006, July 2010.
- [17] M. van der Klis. Millisecond Oscillations in X-ray Binaries. *Annu. Rev. Astron. Astrophys.*, 38:717–760, January 2000.
- [18] J. P. Halpern, K. M. Leighly, and H. L. Marshall. An Extreme Ultraviolet Explorer Atlas of Seyfert Galaxy Light Curves: Search for Periodicity. *Astrophys. J.*, 585(2):665–676, March 2003.
- [19] Jeffrey E. McClintock and Ronald A. Remillard. *Black hole binaries*, volume 39, pages 157–213. Oxford, 2006.
- [20] Marek Gierliński, Matthew Middleton, Martin Ward, and Chris Done. A periodicity of ~1hour in X-ray emission from the active galaxy RE J1034+396. *Nature (London)*, 455(7211):369–371, September 2008.
- [21] Dacheng Lin, Jimmy A. Irwin, Olivier Godet, Natalie A. Webb, and Didier Barret. A ~3.8 hr Periodicity from an Ultrasoft Active Galactic Nucleus Candidate. *ApJ*, 776(1):L10, October 2013.
- [22] W. N. Alston, M. L. Parker, J. Markevičiūtė, A. C. Fabian, M. Middleton, A. Lohfink, E. Kara, and C. Pinto. Discovery of an ~2-h high-frequency X-ray QPO and iron  $K\alpha$  reverberation in



- the active galaxy MS 2254.9-3712. *MNRAS*, 449(1):467–476, May 2015.
- [23] Krista Lynn Smith, Richard F. Mushotzky, Patricia T. Boyd, and Robert V. Wagoner. Evidence for an Optical Low-frequency Quasi-periodic Oscillation in the Kepler Light Curve of an Active Galaxy. *ApJ*, 860(1):L10, June 2018.
- [24] P. Zhang, J. Z. Yan, and Q. Z. Liu. Two Quasi-periodic Oscillations in ESO 113-G010. *Acta Astronomica Sinica*, 61(1):2, January 2020.
- [25] Luigi Stella and Mario Vietri. Lense-Thirring Precession and Quasi-periodic Oscillations in Low-Mass X-Ray Binaries. *ApJ*, 492(1):L59–L62, January 1998.
- [26] Luigi Stella and Mario Vietri. kHz quasiperiodic oscillations in low-mass x-ray binaries as probes of general relativity in the strong-field regime. *Phys. Rev. Lett.*, 82:17–20, Jan 1999.
- [27] A. N. Aliev and D. V. Galtsov. Radiation from relativistic particles in nongeodesic motion in a strong gravitational field. *General Relativity and Gravitation*, 13(10):899–912, October 1981.
- [28] A. N. Aliev, D. V. Galtsov, and V. I. Petukhov. Negative Absorption Near a Magnetized Black-Hole - Black-Hole Masers. *Astrophys. Space Sci.*, 124(1):137–157, 1986.
- [29] A. N. Aliev and Valeri P. Frolov. Five-dimensional rotating black hole in a uniform magnetic field: The gyromagnetic ratio. *Phys. Rev. D*, 69(8):084022, April 2004.
- [30] Gabriel Török, Pavel Bakala, Eva Šrámková, Zdeněk Stuchlík, and Martin Urbanec. On Mass Constraints Implied by the Relativistic Precession Model of Twin-peak Quasi-periodic Oscillations in Circinus X-1. *Astrophys. J.*, 714(1):748–757, May 2010.
- [31] Pavel Bakala, Eva Šrámková, Zdeněk Stuchlík, and Gabriel Török. On magnetic-field-induced non-geodesic corrections to relativistic orbital and epicyclic frequencies. *Classical and Quantum Gravity*, 27(4):045001, February 2010.
- [32] Gabriel Török, Pavel Bakala, Eva Šrámková, Zdeněk Stuchlík, Martin Urbanec, and Kateřina Goluchová. Mass-Angular-momentum Relations Implied by Models of Twin Peak Quasi-periodic Oscillations. *Astrophys. J.*, 760(2):138, December 2012.
- [33] Andres F. Gutierrez-Ruiz, Cesar A. Valenzuela-Toledo, and Leonardo A. Pachon. Innermost Stable Circular Orbits and Epicyclic Frequencies Around a Magnetized Neutron Star. *arXiv e-prints*, page arXiv:1309.6396, September 2013.
- [34] Bushra Majeed, Mubasher Jamil, and Saqib Hussain. Particle Dynamics Around Weakly Magnetized Reissner-Nordström Black Hole. *arXiv e-prints*, page arXiv:1411.4811, November 2014.
- [35] Mustapha Azreg-Aïnou. Vacuum and nonvacuum black holes in a uniform magnetic field. *European Physical Journal C*, 76(7):414, July 2016.
- [36] Bobur Turimov, Bobir Toshmatov, Bobomurat Ahmedov, and Zdeněk Stuchlík. Quasinormal modes of magnetized black hole. *Phys. Rev. D*, 100(8):084038, October 2019.
- [37] Ahmadjon Abdujabbarov, Javlon Rayimbaev, Farruh Atamurotov, and Bobomurat Ahmedov. Magnetized Particle Motion in  $\gamma$ -Spacetime in a Magnetic Field. *Galaxies*, 8(4):76, October 2020.
- [38] Miao Yi and Xin Wu. Dynamics of charged particles around a magnetically deformed Schwarzschild black hole. *Phys. Scr.*, 95(8):085008, August 2020.
- [39] Gabriel Török, Andrea Kotrlová, Monika Matuszková, Kateřina Klimovičová, Debora Lančová, Gabriela Urbanecová, and Eva Šrámková. Simple analytic formula relating the mass and spin of accreting compact objects to their rapid X-ray variability. *arXiv e-prints*, page arXiv:2203.04787, March 2022.
- [40] D. Barret, W. Kluźniak, J. F. Olive, S. Paltani, and G. K. Skinner. On the high coherence of kHz quasi-periodic oscillations. *MNRAS*, 357(4):1288–1294, March 2005.
- [41] Didier Barret, Jean-Francois Olive, and M. Coleman Miller. The coherence of kilohertz quasi-periodic oscillations in the X-rays from accreting neutron stars. *MNRAS*, 370(3):1140–1146, August 2006.
- [42] M. A. Abramowicz and W. Kluźniak. A precise determination of black hole spin in GRO J1655-40. *Astron Astroph*, 374:L19–L20, August 2001.
- [43] Wlodek Kluzniak and Marek Artur Abramowicz. Strong-Field Gravity and Orbital Resonance in Black Holes and Neutron Stars — kHz Quasi-Periodic Oscillations (QPO). *Acta Physica Polonica B*, 32(11):3605, November 2001.
- [44] Robert V. Wagoner, Alexander S. Silbergleit, and Manuel Ortega-Rodríguez. “Stable” Quasi-periodic Oscillations and Black Hole Properties from Diskoseismology. *ApJ*, 559(1):L25–L28, September 2001.
- [45] Shoji Kato. Basic Properties of Thin-Disk Oscillations <sup>1</sup>. *PASJ*, 53(1):1–24, February 2001.
- [46] L. Rezzolla, S'i. Yoshida, T. J. Maccarone, and O. Zanotti. A new simple model for high-frequency quasi-periodic oscillations in black hole candidates. *MNRAS*, 344(3):L37–L41, September 2003.
- [47] Robert V. Wagoner. Diskoseismology and QPOs Confront Black Hole Spin. *ApJ*, 752(2):L18, June 2012.
- [48] Z. Stuchlík, A. Kotrlová, and G. Török. Multi-resonance orbital model of high-frequency quasi-periodic oscillations: possible high-precision determination of black hole and neutron star spin. *Astron Astroph*, 552:A10, April 2013.
- [49] Marcio G. B. de Avellar, Oliver Porth, Ziri Younsi, and Luciano Rezzolla. Kilohertz QPOs in low-mass X-ray binaries as oscillation modes of tori around neutron stars - I. *MNRAS*, 474(3):3967–3975, March 2018.
- [50] Bhupendra Mishra, Wlodek Kluźniak, and P. Chris Fragile. Relativistic, axisymmetric, viscous, radiation hydrodynamic simulations of geometrically thin discs. II. Disc variability. *MNRAS*, 497(1):1066–1079, September 2020.
- [51] Shoji Kato and Mami Machida. A possible origin of kilohertz quasi-periodic oscillations in low-mass X-ray binaries. *PASJ*, 72(3):38, June 2020.
- [52] G. Török, K. Goluchová, J. Horák, E. Šrámková, M. Urbanec, T. Pecháček, and P. Bakala. Twin peak quasi-periodic oscillations as signature of oscillating cusp torus. *MNRAS*, 457(1):L19–L23, March 2016.
- [53] A. Kotrlová, E. Šrámková, G. Török, K. Goluchová, J. Horák, O. Straub, D. Lančová, Z. Stuchlík, and M. A. Abramowicz. Models of high-frequency quasi-periodic oscillations and black hole spin estimates in Galactic microquasars. *Astron Astroph*, 643:A31, November 2020.
- [54] R. Geroch. Multipole Moments. II. Curved Space, August 1970.
- [55] R. O. Hansen. Multipole moments of stationary space-times, 1974.
- [56] Hernando Quevedo and Bahram Mashhoon. Exterior gravitational field of a rotating deformed mass, 1985.
- [57] Hernando Quevedo. General static axisymmetric solution of einstein’s vacuum field equations in prolate spheroidal coordinates, May 1989.
- [58] V S Manko. On the description of the external field of a static deformed mass, sep 1990.
- [59] Norman Gürlebeck. Source integrals for multipole moments in static and axially symmetric spacetimes. *Phys. Rev. D*, 90:024041, Jul 2014.

- [60] José P. S. Lemos and Oleg B. Zaslavskii. Black hole mimickers: Regular versus singular behavior. *Phys. Rev. D*, 78:024040, Jul 2008.
- [61] Rajibul Shaikh, Prashant Kocherlakota, Ramesh Narayan, and Pankaj S. Joshi. Shadows of spherically symmetric black holes and naked singularities. *MNRAS*, 482(1):52–64, January 2019.
- [62] M. A. Abramowicz, W. Kluźniak, and J. P. Lasota. No observational proof of the black-hole event-horizon. *Astron Astroph*, 396:L31–L34, December 2002.
- [63] M. Bursa, M. A. Abramowicz, V. Karas, and W. Kluźniak. The Upper Kilohertz Quasi-periodic Oscillation: A Gravitationally Lensed Vertical Oscillation. *ApJ*, 617(1):L45–L48, December 2004.
- [64] Hermann Weyl. Zur gravitationstheorie, 1917.
- [65] David M. Zipoy. Topology of some spheroidal metrics, 1966.
- [66] B. H. Voorhees. Static axially symmetric gravitational fields, Nov 1970.
- [67] Hernando Quevedo. Mass Quadrupole as a Source of Naked Singularities, Jan 2011.
- [68] Shokoufe Faraji. Circular geodesics in a new generalization of q-metric. *Universe*, 8(3), 2022.
- [69] There is a typo in the equation for  $\hat{\gamma}$  in our paper related to the study of unmagnetized case [88].
- [70] Robert M. Wald. Black hole in a uniform magnetic field. *Phys. Rev. D*, 10:1680–1685, Sep 1974.
- [71] M. Yu. Piotrovich, N. A. Silant’ev, Yu. N. Gnedin, and T. M. Natsvlshvili. Magnetic fields and quasi-periodic oscillations of black hole radiation. *Astrophysical Bulletin*, 66(3):320–324, July 2011.
- [72] L. Stella and M. Vietri. Quasi-Periodic Oscillations from Low-Mass X-ray Binaries and Strong Field Gravity. In Riccardo Giacconi, Salvatore Serio, and Luigi Stella, editors, *X-ray Astronomy 2000*, volume 234 of *Astronomical Society of the Pacific Conference Series*, page 213, January 2001.
- [73] For an alternative definition of the epicyclic harmonic motion see [89].
- [74] G. Török, A. Kotrlová, E. Šrámková, and Z. Stuchlík. Confronting the models of 3:2 quasiperiodic oscillations with the rapid spin of the microquasar GRS 1915+105. *Astron Astroph*, 531:A59, July 2011.
- [75] G. Török, M. A. Abramowicz, W. Kluźniak, and Z. Stuchlík. The orbital resonance model for twin peak kHz quasi periodic oscillations in microquasars. *Astron Astroph*, 436(1):1–8, June 2005.
- [76] A. Kotrlová, E. Šrámková, G. Török, Z. Stuchlík, and K. Goluchová. Super-spinning compact objects and models of high-frequency quasi-periodic oscillations observed in Galactic microquasars. II. Forced resonances. *Astron Astroph*, 607:A69, November 2017.
- [77] Martin Kološ, Arman Tursunov, and Zdeněk Stuchlík. Possible signature of the magnetic fields related to quasi-periodic oscillations observed in microquasars. *European Physical Journal C*, 77(12):860, December 2017.
- [78] Marek A. Abramowicz, Włodek Kluzniak, Zdeněk Stuchlík, and Gabriel Török. Twin peak QPOs frequencies in microquasars and Sgr A\*. The resonance and other orbital models. In *RAGtime 4/5: Workshops on black holes and neutron stars*, pages 1–23, December 2004.
- [79] Luigi Stella and Mario Vietri. Strong Field Gravity and Quasi-Periodic Oscillations from Low-Mass X-Ray Binaries. In Vahe G. Gurzadyan, Robert T. Jantzen, and Remo Ruffini, editors, *The Ninth Marcel Grossmann Meeting*, pages 426–437, December 2002.
- [80] A. Čadež, M. Calvani, and U. Kostić. On the tidal evolution of the orbits of low-mass satellites around black holes. *Astron Astroph*, 487(2):527–532, August 2008.
- [81] U. Kostić, A. Čadež, M. Calvani, and A. Gomboc. Tidal effects on small bodies by massive black holes. *Astron Astroph*, 496(2):307–315, March 2009.
- [82] Shoji Kato. Resonant Excitation of Disk Oscillations by Warps: A Model of kHz QPOs. *PASJ*, 56:905–922, October 2004.
- [83] Paweł Lachowicz, Bożena Czerny, and Marek A. Abramowicz. Wavelet analysis of MCG-6-30-15 and NGC 4051: a possible discovery of QPOs in 2:1 and 3:2 resonance. *arXiv e-prints*, pages astro-ph/0607594, July 2006.
- [84] Wen Fu and Dong Lai. Effects of Magnetic Fields on the Diskoseismic Modes of Accreting Black Holes. *Astrophys. J.*, 690(2):1386–1392, January 2009.
- [85] Janosz W. Dewberry, Henrik N. Latter, Gordon I. Ogilvie, and Sebastien Fromang. HFQPOs and discoseismic mode excitation in eccentric, relativistic discs. II. Magnetohydrodynamic simulations. *MNRAS*, 497(1):451–465, September 2020.
- [86] Ronald A. Remillard and Jeffrey E. McClintock. X-Ray Properties of Black-Hole Binaries. *Annu. Rev. Astron. Astrophys.*, 44(1):49–92, September 2006.
- [87] Rebecca Shafee, Jeffrey E. McClintock, Ramesh Narayan, Shane W. Davis, Li-Xin Li, and Ronald A. Remillard. Estimating the Spin of Stellar-Mass Black Holes by Spectral Fitting of the X-Ray Continuum. *ApJ*, 636(2):L113–L116, January 2006.
- [88] Shokoufe Faraji and Audrey Trova. Quasi-periodic oscillatory motion of particles orbiting a distorted, deformed compact object. *Universe*, 7(11), 2021.
- [89] R. M. Wald. *General relativity*. Oxford, 1984.